

# Oxygen Diffusion in Platinum Electrodes: A Molecular Dynamics Study of the Role of Extended Defects

Alexander F. Zurhelle, Wilhelm Stehling, Rainer Waser, Roger A. De Souza, and Stephan Menzel\*

Platinum serves as a model electrode in solid-state electrochemistry and as the inert electrode in redox-based resistive random-access memory (ReRAM) technology. Experimental work has proposed that oxygen may diffuse faster along platinum's extended defects, but quantitative, unambiguous transport data do not exist. In this study, the diffusion of oxygen atoms in crystalline platinum and along its extended defects is studied as a function of temperature by means of molecular dynamics (MD) simulations with the ReaxFF interatomic potentials. The MD simulations indicate that platinum vacancies trap oxygen atoms, inhibiting their diffusion through the platinum lattice and leading to a high activation enthalpy of diffusion of around 3 eV. This picture of trapping is supported by static density-functional-theory calculations. MD simulations of selected dislocations and selected grain boundaries indicate that oxygen diffusion is much faster along these extended defects than through the Pt lattice at temperatures below 1400 K, exhibiting a much lower activation enthalpy of  $\approx 0.7$  eV for all extended defects examined. Producing specific electrode microstructures with controlled densities and types of extended defects thus offers a new avenue to improve the performance of ReRAM devices and to prevent device failure.

## 1. Introduction

Redox-based resistive random-access memory (ReRAM)<sup>[1]</sup> cells typically consist of transition metal oxides sandwiched

between an inert metal electrode and an oxidizable metal electrode, for instance, Pt|TiO<sub>x</sub>|Ti,<sup>[2,3]</sup> Pt|TaO<sub>x</sub>|Ta<sup>[4,5]</sup> and Pt|HfO<sub>x</sub>|Hf.<sup>[6,7]</sup> By applying appropriate voltages, the electrical resistance of ReRAM cells can be changed reversibly between high and low states. Apart from their role as memory devices,<sup>[8]</sup> these devices are also promising candidates for in-memory computing<sup>[9,10]</sup> and neuromorphic computing<sup>[11]</sup> due to their tunable resistivity.<sup>[12,13]</sup>

The platinum electrodes in such cells are usually considered inert, but there are two ways in which they may crucially affect the characteristics of ReRAM devices: First, most ReRAM cells require an initial electroforming step, which can be performed by applying a positive voltage to a platinum electrode.<sup>[14–20]</sup> During this process, a conductive filament or region is created by removing oxygen from the oxide. Second, the switching mechanism of ReRAM cells with anomalous

(or eightwise) *I*–*V* characteristics<sup>[21]</sup> has recently been linked to oxygen exchange at the Pt|oxide interface.<sup>[3,22,23]</sup> In both cases, the removed oxygen will either diffuse through the electrode or form bubbles between electrode and oxide. This can influence devices and their characteristics in multiple ways: Bubble formation can delaminate the interface, and thereby cause device failure.<sup>[14]</sup> If oxygen is removed too far from the interface, it cannot be reincorporated and the device will be stuck in a low-resistive state. Furthermore, the unwanted occurrence of eightwise resistive switching at Pt|oxide interfaces is a failure mechanism for ReRAM cells with normal (counter-eightwise) *I*–*V* characteristics,<sup>[5,23,24]</sup> and such a coexistence of opposing switching mechanisms has been observed in several systems.<sup>[3,16,17,19,20,22,25–30]</sup> For ReRAM cells, where the initial electroforming occurred at the Pt|oxide interface, oxygen transport into the platinum electrode is likely to impact the size and the shape of the filament and thereby the device characteristics.


Platinum also often serves as electrode material in the field of solid-state electrochemistry, for example, in oxygen sensors or as model cathode in solid-oxide fuel cells.<sup>[31–41]</sup> Here, too, oxygen transport through platinum electrodes can determine the reaction rate.<sup>[31,37–39]</sup>

Oxygen diffusion in platinum has been studied both experimentally<sup>[37,42–47]</sup> and computationally,<sup>[48]</sup> but the picture that

A. F. Zurhelle, W. Stehling, R. Waser  
Institute of Electronic Materials (IWE 2)  
RWTH Aachen University  
52074 Aachen, Germany

R. Waser, S. Menzel  
Peter Grünberg Institute 7  
Forschungszentrum Jülich GmbH and JARA-FIT  
52425 Jülich, Germany  
E-mail: st.menzel@fz-juelich.de

R. A. De Souza  
Institute of Physical Chemistry (IPC)  
RWTH Aachen University  
52074 Aachen, Germany

 The ORCID identification number(s) for the author(s) of this article can be found under <https://doi.org/10.1002/admi.202101257>.

© 2021 The Authors. Advanced Materials Interfaces published by Wiley-VCH GmbH. This is an open access article under the terms of the Creative Commons Attribution License, which permits use, distribution and reproduction in any medium, provided the original work is properly cited.

DOI: 10.1002/admi.202101257

**Table 1.** Cohesive energy of Pt, formation energy of Pt vacancies, O<sub>2</sub> bond energy, incorporation energies of oxygen ( $\Delta E_{\text{inc}}$ ) onto various sites in platinum, and activation barriers ( $\Delta E^\ddagger$ ) for interstitial oxygen migration, substitutional oxygen migration, oxygen detrapping, and vacancy migration in crystalline platinum. See Table S1, Supporting Information, for energies calculated with DFT-D3 dispersion correction.<sup>[65,66]</sup>

	ReaxFF (this work)	DFT-PBE (this work)	DFT-PW91 (Stumpf et al. <sup>[48]</sup> )	Exp. data	Reaction
$\Delta E_{\text{Pt,cohesion}}$ [eV]	−5.77	−5.49		−5.86 <sup>[56]</sup>	Pt (g) → Pt (s)
$\Delta E_{\text{vac}}$ [eV]	2.72	0.69	0.73	1.3 to 1.7 <sup>[57,58]</sup>	$\emptyset \rightarrow v_{\text{Pt}}$
$\Delta E_{\text{O}_2}$ [eV]	−2.69	−3.04	−4.91 <sup>a)</sup>	−2.58 <sup>[56]</sup>	O (g) → ½ O <sub>2</sub> (g)
$\Delta E_{\text{inc}}(\text{O}_{\text{i,octahedral}})$ [eV]	1.99	3.20	2.95		½ O <sub>2</sub> (g) → O <sub>i,octahedral</sub>
$\Delta E_{\text{inc}}(\text{O}_{\text{i,tetrahedral}})$ [eV]	4.69	1.52	1.46		½ O <sub>2</sub> (g) → O <sub>i,tetrahedral</sub>
$\Delta E_{\text{inc}}(\text{O}_{\text{Pt,centered}})$ [eV]	2.64	1.93	1.75		½ O <sub>2</sub> (g) + v <sub>Pt</sub> → O <sub>Pt,centered</sub>
$\Delta E_{\text{inc}}(\text{O}_{\text{Pt,displaced}})$ [eV]	0.52	0.47			½ O <sub>2</sub> (g) + v <sub>Pt</sub> → O <sub>Pt,displaced</sub>
$\Delta E^\ddagger_{\text{mig}}(\text{O})$ [eV]	1.99	1.67	1.49		O <sub>i</sub> → O <sub>i</sub> <sup>TS</sup>
$\Delta E^\ddagger_{\text{mig}}(\text{O}_{\text{Pt,displaced}})$ [eV]	3.28	2.65			O <sub>Pt,displ.</sub> → O <sub>Pt</sub> <sup>TS</sup>
$\Delta E^\ddagger_{\text{detrapp}}(\text{O}_{\text{Pt,displaced}})$ [eV]	3.34	2.50			O <sub>Pt,displ</sub> → {v <sub>Pt</sub> -O <sub>i</sub> } <sup>TS</sup>
$\Delta E^\ddagger_{\text{mig}}(\text{v}_{\text{Pt}})$ [eV]	2.45	1.21		1.1 to 1.5 <sup>[57]</sup>	v <sub>Pt</sub> → {v <sub>Pt</sub> -Pt <sub>i</sub> -v <sub>Pt</sub> } <sup>TS</sup>

a) Only the value relative to the spin-averaged oxygen atom was given. <sup>TS</sup>Transition state

emerges is far from clear. Indeed, of the experimental studies of oxygen diffusion in platinum,<sup>[42–44]</sup> only Velho and Bartlett<sup>[44]</sup> were able to detect oxygen diffusion, and thus, determine chemical diffusion coefficients of oxygen in platinum (and even this, only at elevated temperatures around 1750 K). They were unable, however, to convert their chemical diffusion coefficients into tracer diffusion coefficients. Furthermore, the defect structures of the samples they investigated (in terms of vacancy, dislocation, and grain-boundary densities) were not reported. It is unclear, therefore, which diffusion path was examined in their transport measurements.

This is a critical point, for several reports propose fast oxygen diffusion along extended defects in platinum,<sup>[37,45–47]</sup> and only rough estimations of diffusion coefficients are available.<sup>[46]</sup> DFT calculations by Stumpf et al. yielded an activation barrier of 0.7 eV for oxygen migration along the  $\Sigma 5(310)[001]$  symmetric tilt grain boundary,<sup>[48]</sup> compared with a value of 1.49 eV for oxygen migration through the lattice.

In this study, we use atomistic methods to investigate how fast oxygen moves in the platinum lattice and how fast it moves along extended defects in platinum. To this end, we performed defect energy and nudged-elastic-band (NEB) calculations, as well as molecular dynamics (MD) simulations of oxygen diffusion through crystalline platinum and along its extended defects. With such knowledge, we discuss how oxygen transport through platinum electrodes can influence the characteristics of ReRAM cells.

## 2. Results and Discussion

First, we present energy calculations for oxygen defects in the platinum lattice, followed by static calculations of the migration barriers for these defects. Next, we move on to MD simulations of oxygen diffusion through platinum and then at extended defects. After presenting these results, we discuss their implications for ReRAM cells.

### 2.1. Static Calculations: Defect Energies

We examined a number of processes concerning oxygen in platinum using two methods: interatomic potentials (ReaxFF)<sup>[49,50]</sup> and DFT<sup>[51–55]</sup> calculations (with the PBE functional). **Table 1** summarizes our results. Literature data from experiments<sup>[56–58]</sup> and data from the previous DFT study<sup>[48]</sup> by Stumpf et al. based on the PW91 functional<sup>[59]</sup> are provided for comparison.

We consider first three energies for which experimental data for comparison exist. Values of the cohesive energy of Pt calculated by the two methods are in good agreement with each other and with literature data.<sup>[56]</sup> The calculated formation energy of Pt vacancies  $\Delta E_{\text{vac}}$  is, relative to the range of experimental values,<sup>[57,58]</sup> strongly overestimated by ReaxFF but underestimated by DFT-PBE. This underestimation has previously been addressed in the literature by Mattsson and Mattson, who, applying a surface error correction (they reasoned that a vacancy in a metal resembles an internal surface), arrived at  $\Delta E_{\text{vac}} = 1.16$  eV, a value much closer, though still lower, than experimental values.<sup>[60,61]</sup> Lastly, the oxygen bond energy  $\Delta E_{\text{O}_2}$  is only slightly overestimated with ReaxFF and more overestimated with DFT-PBE, compared with values from experiment. Since Stumpf et al. only provide the energy relative to spin-averaged oxygen atoms, a direct comparison with this value is not possible.

Moving onto the incorporation of oxygen from the gas phase into Pt, we investigated the energy of oxygen at different sites within the platinum crystal, in order to determine the preferred sites (with only the DFT-PW91 results of Stumpf et al. available for comparison). For the incorporation of an oxygen atom from an oxygen molecule onto an interstitial site, the results obtained with ReaxFF and DFT-PBE disagree: While the ReaxFF calculations predict that oxygen prefers the octahedral to the tetrahedral site (1.99 eV versus 4.69 eV), the DFT-PBE results indicate the opposite (3.20 eV versus 1.52 eV). Both methods agree, however, that the preferred mode of incorporation from an oxygen molecule is into a platinum vacancy, with relatively similar energies of 0.52 eV (ReaxFF) and 0.47 eV (DFT-PBE). It is noteworthy that with both methods two different oxygen positions

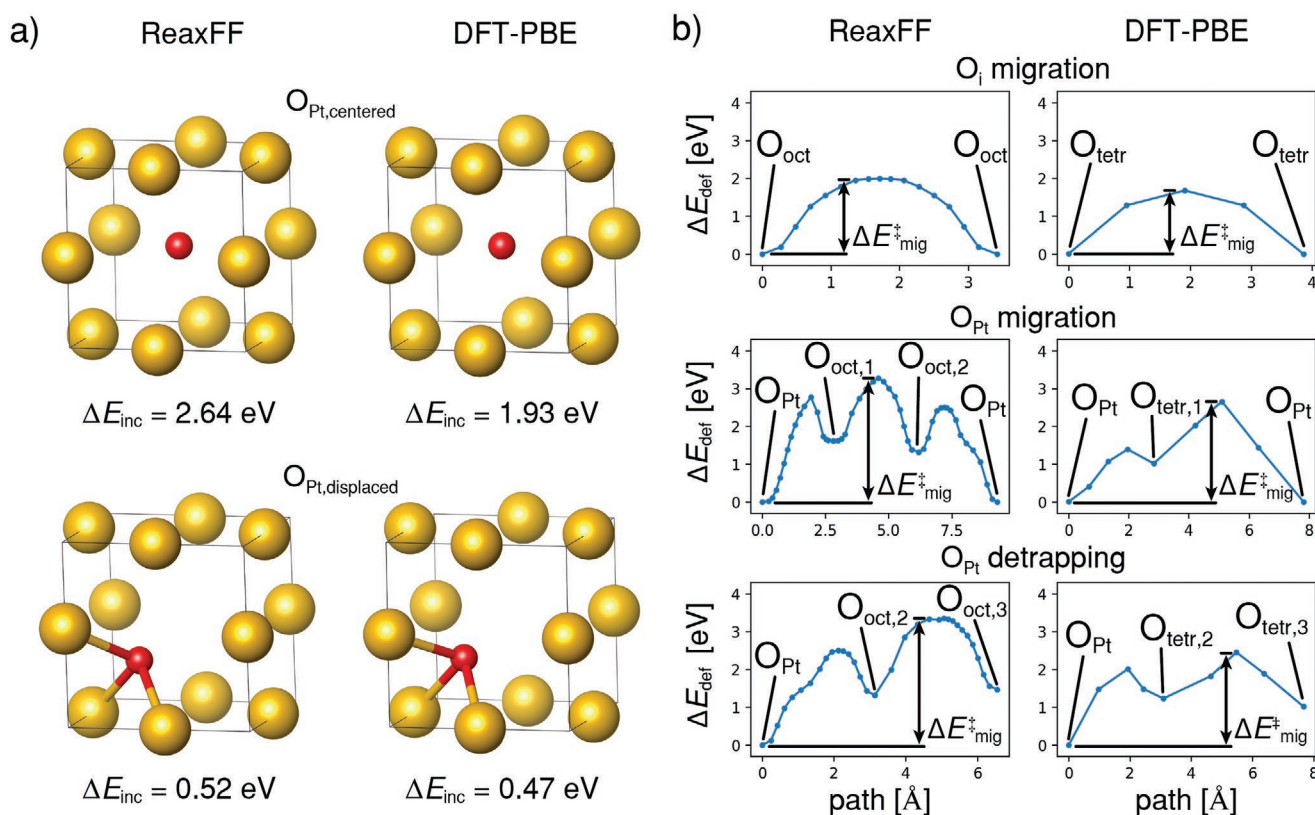


**Figure 1.** a) Incorporation energies  $\Delta E_{inc}$  for an oxygen atom at a Pt vacancy, calculated with ReaxFF and DFT-PBE for two sites — in the center of the Pt vacancy and the minimum energy position, where the oxygen atom is displaced towards three Pt atoms. Images are rendered with VESTA.<sup>[64]</sup> b) Migration barriers for interstitial oxygen diffusion, substitutional oxygen diffusion, and the barrier for oxygen detrapping from the platinum vacancy, calculated with the climbing-image nudged elastic band method. The according structures are shown in Figure S2, Supporting Information.

at a platinum vacancy can be distinguished (see **Figure 1a**). At the very center of a platinum vacancy, the energy is higher than at the preferred, off-center site, for which the oxygen atom is displaced towards three platinum atoms. The energy landscape of an oxygen atom in crystalline platinum predicted by ReaxFF is shown in Figure S1, Supporting Information.

Earlier work by Stumpf et al., using DFT-PW91 calculations, arrived at very similar results, but with lower energies for the interstitial defects: 2.95 eV for the octahedral interstitial and 1.46 eV for the tetrahedral interstitial. The energy they obtained for an oxygen atom at a platinum vacancy (substitutional defect), however, only agrees well with the energy that we calculated for the position at center of the platinum vacancy, which according to our calculations is not the minimum energy position. As a consequence, Stumpf et al. predicted incorrectly that the tetrahedral site is the most favorable one for oxygen in bulk platinum. Further differences between the energies calculated in this work and the results of Stumpf et al. can be attributed to the different computational approaches: While we used the PBE functional and the projector augmented wave (PAW) method with an energy cutoff of 400 eV, Stumpf et al. used the PW91 functional and ultrasoft pseudopotentials (USPP) with an energy cutoff of 270 eV. In general, the PAW method is considered to yield better results than calculations employing USPP.

Thus, our defect energies (shown in Table 1) indicate that oxygen will be preferentially present as a substitutional defect in Pt. If oxygen is present as an interstitial defect, it will to some

degree become trapped if it meets a Pt vacancy. The degree to which trapping takes place and thus how the macroscopic diffusion of oxygen is affected depends on the availability of Pt vacancies, the energy barriers for trapping and detrapping, as well as the migration barriers for interstitial and substitutional oxygen diffusion. These are considered in the next section.

## 2.2. Static Calculations: Migration Barriers

Figure 1b shows energy profiles for the migration of oxygen in Pt determined with ReaxFF and DFT-PBE using the climbing-image nudged elastic band method (CI-NEB).<sup>[62,63]</sup> From these profiles, we extracted the migration barriers,  $\Delta E_{mig}^\ddagger$  (values given in Table 1). For the interstitial diffusion of oxygen through crystalline platinum, ReaxFF predicts an energy barrier of 1.99 eV. Here, the oxygen atom moves from one octahedral site to an adjacent one, passing between two platinum atoms that form the common edge of the edge-sharing octahedra. Our DFT-PBE calculations predict that the interstitial migration occurs from tetrahedral site to tetrahedral site passing through an octahedral site with a barrier of 1.67 eV. Because the oxygen atom at the octahedral site resembles the transition state of this migration process, we can extract the migration barrier from the data of Stumpf et al. by calculating the difference between the tetrahedral and octahedral interstitial energies. This yields a slightly lower migration barrier of 1.49 eV.

The oxygen migration processes involving substitutional oxygen atoms show significantly larger activation barriers. We distinguish between two different migration processes: The first is substitutional diffusion, where the oxygen atom moves from one platinum vacancy to another. The second is detrapping, where the oxygen atom escapes the platinum vacancy and is free to migrate as an interstitial defect. (A detailed description of these processes is given in Figure S2, Supporting Information.) With ReaxFF, the activation energy for substitutional diffusion is 3.28 eV and for detrapping 3.34 eV. DFT-PBE predicts these energies to be 2.65 and 2.50 eV, respectively. That is, the oxygen migration barriers predicted by DFT-PBE are lower than those predicted by ReaxFF (by up to 0.84 eV). Both methods, however, indicate that interstitial oxygen diffusion has a significantly lower activation energy than the two processes involving substitutional oxygen, around 1.3 eV (DFT-PBE) and 0.9 eV (ReaxFF). Consequently, interstitial oxygen will diffuse faster through crystalline platinum than substitutionally dissolved oxygen. Furthermore, with both methods, the energy barriers for substitutional oxygen diffusion and oxygen detrapping are very similar (within 0.2 eV from each other). As oxygen detrapping results in fast diffusing oxygen interstitials, it can be expected to play an important role in oxygen diffusion.

Since the substitutional diffusion path requires a large number of mobile Pt vacancies, we have also calculated migration barriers for platinum vacancies. While the DFT-PBE result of 1.21 eV agrees well with measured values<sup>[57]</sup> that range from 1.1 to 1.5 eV, ReaxFF strongly overestimates this migration barrier with 2.45 eV. Thus, the effects of Pt vacancy diffusion may be underestimated in ReaxFF-based MD simulations. (The effects of Pt vacancy diffusion may nevertheless be correctly reproduced in ReaxFF-based MD simulations, since there seems to be a difference between the static and MD results, differences that we attribute to finite-temperature effects, see next section.)

The calculated activation barriers for migration and detrapping suggest that an interstitial oxygen atom travels rapidly through the platinum lattice until it meets a Pt vacancy and

becomes trapped as a substitutional defect. Whether oxygen is mainly present as a substitutional or interstitial moiety will also depend, however, on the availability of Pt vacancies, that is, the ratio of Pt vacancies to dissolved oxygen atoms.

### 2.3. MD Simulations: Oxygen Diffusion through the Lattice

We investigated in our MD simulations at a range of temperatures a number of scenarios for oxygen diffusion in crystalline platinum. From the simulations, we extracted the development of the mean squared displacement of oxygen as a function of time (Figure 2a). As linear behavior was observed, we fitted the Einstein equation (see Computational Details) to the data to obtain tracer diffusion coefficients of oxygen in Pt (see Figure 2b).

The first system that we considered is a supercell of crystalline platinum-free from any Pt vacancies with a size of  $15 a \times 15 a \times 15 a$ , where  $a = 3.95 \text{ \AA}$  is the lattice parameter of Pt. 100 oxygen atoms were inserted at random into interstitial sites, resulting in an oxygen concentration of 0.7 at.-%. From the temperature dependence of the diffusion coefficients, we determined an activation enthalpy of  $(1.6 \pm 0.1) \text{ eV}$ . For this determination, we only considered data for temperatures up to 2000 K, because at higher temperatures the data in the Arrhenius plot deviated increasingly from linear behavior. Examination of the simulations suggested that this non-linearity might be caused by oxygen interstitials forming clusters over the course of the simulation. We also note that the activation energy obtained in the MD simulations is lower than the migration energy determined from static calculations with ReaxFF (1.99 eV), but in good agreement with the DFT result of 1.52 eV (see Table 1). This discrepancy between the static ReaxFF and MD values may be the result of oxygen interstitial interactions, but it may also be due to the MD simulations referring to finite temperatures, and thus to different lattice parameters, whereas the static calculation corresponds to  $T = 0 \text{ K}$ . These data, it is emphasized, are important, as they provide a reference against

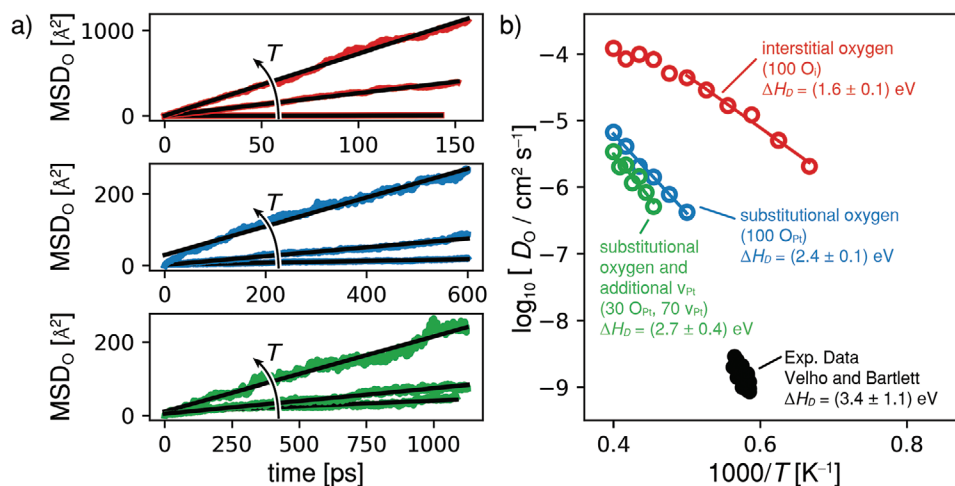


**Figure 2.** a) Mean squared displacement (MSD) of oxygen atoms for three different cases. For each case, the MSD at the highest, one intermediate, and lowest temperature are shown together with a linear fit. From the slopes of these linear fits, diffusion coefficients are determined. b) Oxygen tracer diffusion coefficients (open circles) determined for three different cases compared to chemical diffusion coefficients from experiments (bullets).<sup>[44]</sup>

which the effects of other defects on oxygen diffusion can be studied.

Since Pt at equilibrium at a finite temperature will contain vacancies, and since the static results (Table 1) suggest that the interactions with Pt vacancies are critical, we examined oxygen diffusion in a second system, in which we started with all oxygen atoms placed in Pt vacancies. The 100 Pt vacancies were generated by randomly deleting Pt atoms. In this case, the diffusion of oxygen is orders of magnitudes slower and exhibits a much larger activation enthalpy, of  $(2.4 \pm 0.1)$  eV, than in the previous case. This system is somewhat artificial, though, as it contains exactly as many Pt vacancies as oxygen atoms. Far more likely is that there is an excess of one or the other. If there is an excess of O atoms, oxygen diffusion will take place rapidly by an interstitial mechanism, as examined in the first scenario, since one Pt vacancy will only trap one oxygen atom, thus leaving a large number of freely diffusing oxygen interstitials. The opposite case, an excess of Pt vacancies, was considered in the third scenario.

Specifically, 100 platinum vacancies were placed in a  $15 a \times 15 a \times 15 a$  supercell of platinum, but now only 30 of these vacancies were occupied initially by an oxygen atom. Now, oxygen diffusion is even slower than in the previous scenario, and the activation energy increases to  $(2.7 \pm 0.4)$  eV. The difference in behavior is attributed to the relative availability of empty  $v_{\text{Pt}}$ . In the second scenario, a substitutional oxygen atom, having escaped from the trap of a platinum vacancy, is forced to migrate as a (mobile) interstitial moiety until it encounters one of the very few empty vacancies. In the third scenario, there are many empty  $v_{\text{Pt}}$  traps available. Indeed, further MD simulations (see Figure S3, Supporting Information) confirm that interstitial oxygen atoms are quickly trapped at available platinum vacancies, and then mostly remain trapped throughout the simulation.

Also shown in the Figure are the chemical diffusion coefficients obtained by Velho and Bartlett.<sup>[44]</sup> Assuming that these are equal to the tracer diffusion coefficients, as suggested by Velho and Bartlett, we find acceptable agreement between their data and our data for the third scenario, both in terms of the absolute magnitude and temperature dependence, their value of  $(3.4 \pm 1.1)$  eV according well with our value of  $(2.7 \pm 0.4)$  eV.

It is noteworthy that Velho and Bartlett estimated the concentration of dissolved oxygen to be 0.6 at.-% at 1750 K.<sup>[44]</sup> The concentration of Pt vacancies at this temperature has been determined from specific heat measurements to be around 0.2 at.-%.<sup>[58]</sup> These concentrations suggest an excess of oxygen atoms over Pt vacancies rather than an excess of Pt vacancies that we assumed above. Strictly speaking, however, one would need to know the concentration of Pt vacancies in the samples studied by Velho and Bartlett, and one would also require confirmation of the oxygen concentration reported by Velho and Bartlett. In any case, our simulations clearly indicate a surplus of Pt vacancies relative to dissolved oxygen atoms.

In conclusion, our simulations indicate that trapping at platinum vacancies can significantly reduce the diffusion of oxygen through platinum single crystals. The ratio of dissolved oxygen atoms to available platinum vacancies can therefore strongly influence oxygen transport through crystalline platinum.

## 2.4. MD Simulations: Oxygen Diffusion Along Extended Defects

In order to study the oxygen transport along dislocations in platinum, three small-angle grain boundaries [symmetrical tilt misorientation angles of  $5^\circ$ ,  $6^\circ$ , and  $7^\circ$  around the (001) axis] were constructed. 100 oxygen atoms were placed at random positions along these dislocations. To study the transport along high-angle grain boundaries, five different systems were generated with randomly selected misorientation angles, and then 100 oxygen atoms were placed at these grain boundaries. (Further details on the generation of the extended defects are given in the Computational Methods section.)

The mean squared displacements of oxygen atoms obtained from the MD simulations at  $T = 1500$  K are shown in Figure 3a for two directions, along the extended defects (colored) and perpendicular to them (grey). These data as well as the jump trajectories displayed in Figure 4 demonstrate that significant transport only occurred along the dislocations or grain boundaries, and not perpendicular to them. Thus, diffusion coefficients were calculated for diffusion in one dimension (dislocations) or two dimensions (grain boundaries).

The tracer diffusion coefficients of oxygen obtained in this way are compared in Figure 3b with data obtained for the cells without extended defects (all three scenarios). The transport of oxygen along dislocations or along grain boundaries occurs with very similar diffusion coefficients and, in both cases, with an activation enthalpy of  $(0.7 \pm 0.1)$  eV. This value agrees excellently with the migration barrier of  $(0.7 \pm 0.1)$  eV, determined for one specific grain boundary by Stumpf et al.<sup>[48]</sup> At temperatures below 1400 K, the diffusion along these defects is faster than the transport through the lattice, especially in the presence of platinum vacancies. Extrapolating down to 800 K, we find that diffusion along extended defects is faster than interstitial diffusion by 3 orders of magnitude, and faster than diffusion in the presence of excess platinum vacancies by 9 orders of magnitude.

## 3. Discussion

In this study, we presented ReaxFF and DFT-PBE calculations of the energy of an oxygen atom at different sites in a platinum crystal. Both descriptions appear to have their weaknesses: For example, while ReaxFF strongly overestimates the formation energy for a platinum vacancy, DFT-PBE underestimates this formation energy and overestimates the oxygen bond energy. The most striking discrepancy between ReaxFF and DFT-PBE results is the energy at the different interstitial sites. However, both descriptions also agree on several critical points: They predict the most favorable site for an oxygen atom to be at a platinum vacancy (not at its center but displaced toward three platinum atoms, see Figure 1a) and they agree on the required incorporation energy of around 0.5 eV (see Table 1). Nudged elastic band calculations with both methods showed that the migration barriers for such a substitutional defect and the energy barrier for oxygen detrapping from the platinum vacancy to an interstitial site are at least 0.8 eV larger than the interstitial migration barrier. Furthermore, the activation energy of  $(1.6 \pm 0.1)$  eV for interstitial

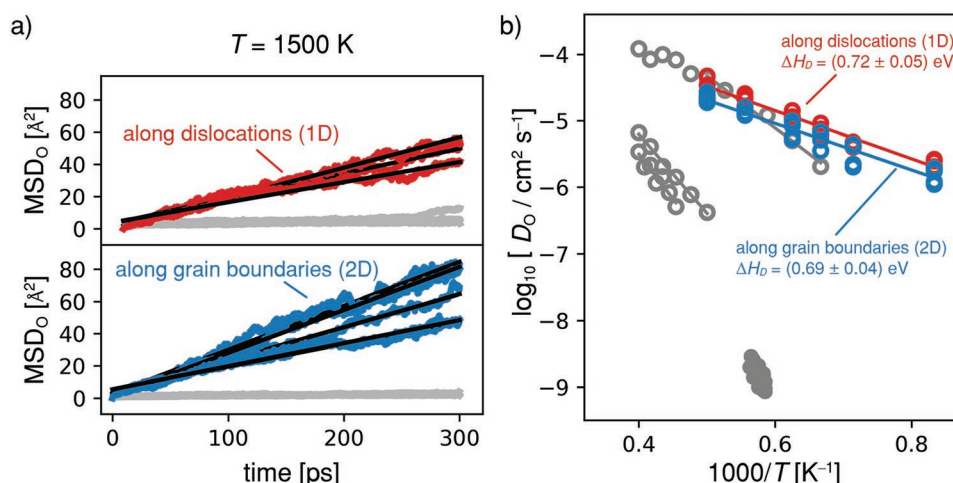


**Figure 3.** a) MSD along extended defects (colored) and perpendicular to them (grey). b) Oxygen diffusion coefficients along extended defects (dislocations: red, grain boundaries: blue). For comparison, the bulk diffusion coefficients from Figure 2 are shown in grey.

diffusion extracted from ReaxFF-based MD simulations is in excellent agreement with the corresponding migration barrier predicted by the DFT-PBE nudged elastic band calculations (see Figure 2b and Table 1). The same applies to the activation energies of  $(2.4 \pm 0.1) \text{ eV}$  and  $(2.7 \pm 0.4) \text{ eV}$  for substitutional diffusion determined from the MD simulations and the corresponding migration barriers calculated with DFT-PBE. Furthermore, the activation energies of about 0.7 eV for oxygen diffusion along several grain boundaries and dislocations agree well with the migration barrier of  $(0.7 \pm 0.1) \text{ eV}$  determined for a specific grain boundary in a previous DFT-PW91 study by Stumpf et al.<sup>[48]</sup> Consequently, the

discrepancies between ReaxFF and DFT calculations apparently do not affect the key messages of this work.

For platinum electrodes, our results indicate that oxygen diffuses orders of magnitudes slower through crystalline platinum, if platinum vacancies are present. It is noteworthy that the situation might be very different microscopically: It is conceivable that oxygen atoms incorporated into platinum at an interface, for example, during reactions in solid-oxide fuel cells or in resistive switching cells, will be incorporated interstitially and, until they meet an empty platinum vacancy, be transported much faster than macroscopic measurements of the diffusion coefficient suggest. Furthermore, locally high concentrations of

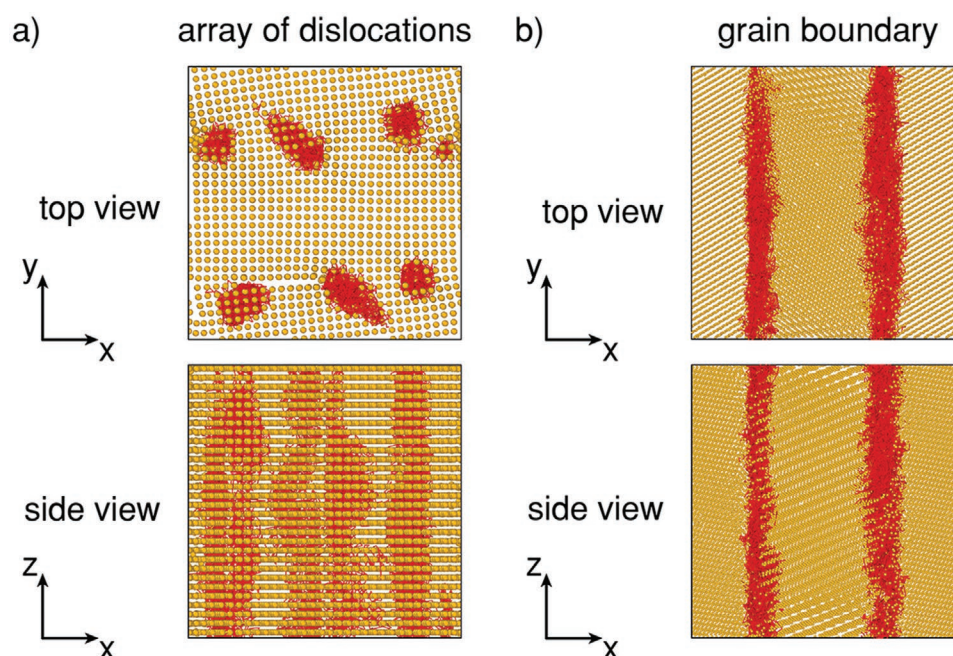


**Figure 4.** Oxygen trajectories (red) for 100 oxygen atoms placed at a) dislocations, b) grain boundaries in platinum over a simulation time of 400 ps at 2000 K. These images are rendered with OVITO.<sup>[67]</sup>

dissolved oxygen atoms could saturate the platinum vacancies preventing further oxygen trapping.

As oxygen transport occurs much faster at extended defects in platinum electrodes, adjusting the microstructure of electrodes during preparation might offer new opportunities to engineer ReRAM cells. Extended defects such as dislocations could be used to influence the position at which the filament is formed in the oxide, for example, to avoid filament formation at the cell boundary. An increased concentration of extended defects in the platinum electrode, for example, through a smaller grain size, could accelerate the removal of oxygen from the interface to mitigate bubble formation or to allow the formation of more oxygen vacancies in the oxide, creating a larger conductive filament and decreasing the resistance of the low-resistive state. Transporting oxygen away from the interface could also lead to a more stable low-resistive state. On the other hand, this might entirely prevent the reincorporation of oxygen into the oxide, and thereby the reset of the device to the high-resistive state. Lowering the concentration of extended defects in the platinum electrode could suppress the oxygen exchange at the Pt|oxide interface, and thus prevent the occurrence of anomalous (eightwise) switching in cells with a different (counter eightwise) switching mechanism.

## 4. Conclusions

We presented static calculations (defect energies and nudged elastic band) and MD simulations to arrive at a far clearer picture of oxygen diffusion through platinum electrodes. Defect energy calculations showed that oxygen atoms prefer to reside at platinum vacancies. This contradicts previous DFT work,<sup>[48]</sup> possibly because a configuration with lower symmetry was not investigated. While we arrive at a similar energy, when the oxygen atoms reside in the center of the Pt vacancy, we find a lower energy for a configuration, in which the oxygen atom is displaced away from the cube center towards three of the surrounding Pt atoms.

Nudged elastic band calculations yielded large activation barriers for substitutional oxygen diffusion (above 2.65 eV) and oxygen detrapping (above 2.50 eV) from the platinum vacancy into interstitial sites. The migration barrier for interstitial oxygen atoms was found to be more than 0.8 eV lower. MD simulations of oxygen transport through crystalline platinum yielded diffusion coefficients with an activation energy of  $(1.6 \pm 0.1)$  eV for interstitial oxygen, and above  $(2.4 \pm 0.1)$  eV for substitutional oxygen. Together with chemical diffusion coefficients measured by Velho et al.,<sup>[44]</sup> this suggests that trapping of oxygen atoms at platinum vacancies significantly limits oxygen diffusion through crystalline platinum.

From MD simulations of oxygen transport at extended defects in platinum, we determined an activation energy of  $(0.7 \pm 0.1)$  eV for oxygen diffusion along both, dislocations and grain boundaries. This is in excellent agreement with the migration barrier for oxygen calculated for one specific grain boundary in a previous DFT study.<sup>[48]</sup> The diffusion coefficients determined in this work show that the oxygen diffusion along these extended defects occurs orders of magnitudes faster than the transport through the lattice. Furthermore, these diffusion

coefficients enable the simulation of oxygen transport through platinum electrodes under consideration of the electrode microstructure, which could improve models of ReRAM devices as well as other electrochemical cells.

Finally, we suggest that engineering the microstructure of platinum electrodes, for example, by creating defects at selected locations or by influencing the density of defects, might improve ReRAM characteristics, for example, by stabilizing the low-resistive state or preventing device failure.

## 5. Experimental Section

**Static Calculations (Defect Energies and Nudged Elastic Band):** For the interatomic potential calculations, we used the ReaxFF potential<sup>[49]</sup> as implemented<sup>[68,69]</sup> in the LAMMPS software package.<sup>[70]</sup> The ReaxFF potential used here was parameterized by Fantauzzi et al. to specifically describe Pt–Pt and Pt–O interactions by fitting the energies and structures for several platinum and platinum oxide bulk phases as well as surface structures to DFT-PBE data.<sup>[50]</sup> This potential was then applied on oxygen surface diffusion and oxygen adsorption on platinum as well as the oxidation of platinum surfaces.<sup>[50,71,72]</sup> Relaxation of crystalline platinum yielded the lattice parameter  $a$  as 3.947 Å. Defect structures were created by placing the defect in a  $5a \times 5a \times 5a$  supercell of crystalline platinum and then relaxing all atomic positions and the cell volumes without symmetry constraints. Migration barriers were determined by performing climbing image nudged elastic band (CI-NEB)<sup>[62,63]</sup> calculations with 15 images. All optimizations continued until all forces were below  $0.05 \text{ eV Å}^{-1}$ . The convergence with respect to the supercell size was checked.

For the electronic structure calculations, we performed DFT-PBE<sup>[51]</sup> calculations with the Vienna Ab Initio Simulation Package (VASP)<sup>[52–54]</sup> and the PAW method<sup>[55]</sup> (cutoff energy of 400 eV for energy calculations and 520 eV for force calculations, valence electron configurations: Pt  $6s^1 5d^9$ , O  $2s^2 2p^4$ ). For the single oxygen and platinum atoms as well as the oxygen molecule, spin-polarized calculations were performed with rectangular cuboid cells (edge lengths around 10 Å). Apart from the single atom calculations, which were performed at the gamma point only, all DFT calculations were carried out on a  $7 \times 7 \times 7$  gamma-centered Monkhost–Pack k-point grid<sup>[73]</sup> with Gaussian smearing with 10 meV. The convergence criterion for the electronic structure was an energy difference of 0.1 meV. Relaxation of crystalline platinum yielded the lattice parameter  $a$  as 3.968 Å. The defects were placed in  $2a \times 2a \times 2a$  supercells of crystalline platinum; all atomic positions and the cell volume were relaxed without symmetry constraints. CI-NEB calculations were performed with 3 images and variable cell parameters. All optimizations were continued until all forces were below  $0.01 \text{ eV Å}^{-1}$ .

**MD Simulations:** MD simulations were performed using LAMMPS and the ReaxFF potential as described above. For bulk structures,  $15a \times 15a \times 15a$  supercells of crystalline platinum were generated with different numbers of platinum vacancies. To investigate the oxygen transport along extended defects, systems were generated with the “polycrystal” mode of AtomsK.<sup>[74]</sup> For dislocations, small-angle grain boundaries were constructed by placing two grains with a misorientation angle of  $5^\circ$ ,  $6^\circ$ , or  $7^\circ$  around the (001) axis into a simulation cell with a size similar to the bulk systems. Due to the periodic boundary conditions, this resulted in two grain boundaries with an array of dislocations. Similarly, large-angle grain boundaries were created with five random sets of misorientation angles (see Supporting Information) along all directions. In these five structures, the periodic boundary conditions also lead to two grain boundaries each. Oxygen atoms were placed at different sites in these systems. All atomic positions and the lattice parameters were then optimized. Subsequently, MD simulations were performed with a time step of 1 fs. The structures were equilibrated for at least 100 ps in the NpT ensemble with a pressure of  $p = 1 \text{ bar}$

and at different temperatures  $T$ , ranging from 1200 to 2500 K. Then, the mean squared displacement of oxygen atoms  $\text{MSD}_\text{O}$  was recorded for at least 150 ps. For temperatures above the melting point of platinum, the crystallinity of the simulated platinum was checked visually and by checking the radial-distribution function for long-range order.

**Oxygen Diffusion Coefficients:** The time dependence of the  $\text{MSD}_\text{O}$  was then linearly fitted. According to the Einstein equation

$$D_\text{O}^* = \frac{1}{2N_\text{dim}} \frac{d\text{MSD}_\text{O}}{dt} \quad (1)$$

the oxygen diffusion coefficient was obtained from the slope of this linear fit. In this equation,  $N_\text{dim}$  denotes the number of dimension along which diffusion occurs: equal to 1 for dislocations, 2 for grain boundaries, and 3 for bulk diffusion.

## Supporting Information

Supporting Information is available from the Wiley Online Library or from the author.

## Acknowledgements

The authors gratefully acknowledge the computing time granted through JARA on the supercomputer JURECA<sup>[75]</sup> at Forschungszentrum Jülich within project JG170. This work was supported by the Deutsche Forschungsgemeinschaft (DFG) within the framework of the collaborative research center “Nanoswitches” (SFB917).

Open access funding enabled and organized by Projekt DEAL.

## Conflict of Interest

The authors declare no conflict of interest.

## Data Availability Statement

The data that support the findings of this study are available from the corresponding author upon reasonable request.

## Keywords

density functional theory diffusion, extended defects, molecular dynamics nudged elastic band oxygen, platinum

Received: July 23, 2021

Revised: October 12, 2021

Published online: December 2, 2021

- [1] R. Waser, R. Dittmann, G. Staikov, K. Szot, *Adv. Mater.* **2009**, *21*, 2632.
- [2] G. Kim, J. Lee, Y. Ahn, W. Jeon, S. Song, J. Seok, J. Yoon, K. Yoon, T. Park, C. Hwang, *Adv. Funct. Mater.* **2013**, *23*, 1440.
- [3] H. Zhang, S. Yoo, S. Menzel, C. Funck, F. Cueppers, D. J. Wouters, C. S. Hwang, R. Waser, S. Hoffmann-Eifert, *ACS Appl. Mater. Interfaces* **2018**, *10*, 29766.
- [4] J. J. Yang, M. Zhang, J. P. Strachan, F. Miao, M. D. Pickett, R. D. Kelley, G. Medeiros-Ribeiro, R. S. Williams, *Appl. Phys. Lett.* **2010**, *97*, 232102/1.
- [5] W. Kim, S. Menzel, D. J. Wouters, Y. Guo, J. Robertson, B. Rösger, R. Waser, V. Rana, *Nanoscale* **2016**, *8*, 17774.
- [6] A. Hardtdegen, C. La Torre, H. Zhang, C. Funck, S. Menzel, R. Waser, S. Hoffmann-Eifert, presented at *2016 IEEE 8th Int. Memory Workshop (IMW)*, Peris **2016**, pp. 1–4.
- [7] S. Kumar, Z. Wang, X. Huang, N. Kumari, N. Davila, J. P. Strachan, D. Vine, A. L. D. Kilcoyne, Y. Nishi, R. S. Williams, *ACS Nano* **2016**, *10*, 11205.
- [8] R. Waser, M. Aono, *Nat. Mater.* **2007**, *6*, 833.
- [9] M. Le Gallo, A. Sebastian, R. Mathis, M. Manica, H. Giefers, T. Tuma, C. Bekas, A. Curioni, E. Eleftheriou, *Nat. Electron.* **2018**, *1*, 246.
- [10] D. Ielmini, H. P. Wong, *Nat. Electron.* **2018**, *1*, 333.
- [11] G. Indiveri, B. Linares-Barranco, R. Legenstein, G. Deligeorgis, T. Prodromakis, *Nanotechnology* **2013**, *24*, 384010.
- [12] D. Kuzum, S. Yu, H.-S. P. Wong, *Nanotechnology* **2013**, *24*, 382001.
- [13] G. W. Burr, R. M. Shelby, A. Sebastian, S. Kim, S. Kim, S. Sidler, K. Virwani, M. Ishii, P. Narayanan, A. Fumarola, L. L. Sanches, I. Boybat, M. Le Gallo, K. Moon, J. Woo, H. Hwang, Y. Leblebici, *Adv. Phys.: X* **2017**, *2*, 89.
- [14] J. J. Yang, F. Miao, M. D. Pickett, D. A. A. Ohlberg, D. R. Stewart, C. N. Lau, R. S. Williams, *Nanotechnology* **2009**, *20*, 215201.
- [15] C. Nauenheim, C. Kuegeler, A. Ruediger, R. Waser, *Appl. Phys. Lett.* **2010**, *96*, 122902.
- [16] D. S. Jeong, H. Schroeder, R. Waser, *Phys. Rev. B* **2009**, *79*, 195317/1.
- [17] F. Miao, J. J. Yang, J. Borghetti, G. Medeiros-Ribeiro, R. S. Williams, *Nanotechnology* **2011**, *22*, 254007.
- [18] K. Skaja, C. Bäumer, O. Peters, S. Menzel, M. Moors, H. Du, M. Bornhöft, C. Schmitz, C.-L. Jia, C. M. Schneider, J. Mayer, R. Waser, R. Dittmann, *Adv. Funct. Mater.* **2015**, *25*, 7154.
- [19] R. Muenstermann, T. Menke, R. Dittmann, R. Waser, *Adv. Mater.* **2010**, *22*, 4819.
- [20] R. Dittmann, R. Muenstermann, I. Krug, D. Park, T. Menke, J. Mayer, A. Besmehn, F. Kronast, C. M. Schneider, R. Waser, *Proc. IEEE* **2012**, *100*, 1979.
- [21] R. Waser, R. Bruchhaus, S. Menzel, in *Redox-Based Resistive Random Access Memories*, 3rd eds., (Ed: R. Waser), Wiley-VCH, Weinheim, Germany **2012**, Ch. 30.
- [22] D. Cooper, C. Baeumer, N. Bernier, A. Marchewka, C. La Torre, R. E. Dunin-Borkowski, S. Menzel, R. Waser, R. Dittmann, *Adv. Mater.* **2017**, *29*, 1700212.
- [23] A. Schoenhals, A. Kindsmueller, C. La Torre, H. Zhang, S. Hoffmann-Eifert, S. Menzel, R. Waser, D. J. Wouters, *Memory Workshop (IMW)*, *2017 IEEE International*, IEEE, Piscataway, NJ **2017**.
- [24] C. La Torre, A. F. Zurhelle, T. Breuer, R. Waser, S. Menzel, *IEEE Trans. Electron Devices* **2019**, *66*, 1268.
- [25] L. Goux, P. Czarnecki, Y. Y. Chen, L. Pantisano, X. P. Wang, R. Degraeve, B. Govoreanu, M. Jurczak, D. J. Wouters, L. Altimime, *Appl. Phys. Lett.* **2010**, *97*, 243509.
- [26] H. Tian, H.-Y. Chen, G. Gao, S. Yu, J. Liang, Y. Yang, D. Xie, J. F. Kang, T.-L. Ren, Y. Zhang, H.-S. P. Wong, *Nano Lett.* **2013**, *13*, 651.
- [27] M. Moors, K. K. Adepalii, Q. Lu, A. Wedig, C. Bäumer, K. Skaja, B. Arndt, H. L. Tuller, R. Dittmann, R. Waser, B. Yildiz, I. Valov, *ACS Nano* **2016**, *10*, 1481.
- [28] Y. S. Kim, J. Kim, M. J. Yoon, C. H. Sohn, S. B. Lee, D. Lee, B. C. Jeon, H. K. Yoo, T. W. Noh, A. Bostwick, E. Rotenberg, J. Yu, S. D. Bu, B. S. Mun, *Appl. Phys. Lett.* **2014**, *104*, 13501/1.
- [29] M. Kubicek, R. Schmitt, F. Messerschmitt, J. L. M. Rupp, *ACS Nano* **2015**, *9*, 10737.
- [30] X. Sun, G. Li, L. Chen, Z. Shi, W. Zhang, *Nanoscale Res. Lett.* **2011**, *6*, 599/1.
- [31] R. Brook, W. Pelzmann, F. Kröger, *J. Electrochem. Soc.* **1971**, *118*, 185.
- [32] P. Fabry, M. Kleitz, *J. Electroanal. Chem. Interfacial Electrochem.* **1974**, *57*, 165.
- [33] J. Fouletier, H. Seiner, M. Kleitz, *J. Appl. Electrochem.* **1974**, *4*, 305.

- [34] E. Schouler, M. Kleitz, *J. Electrochem. Soc.* **1987**, 134, 1045.
- [35] R. Baker, J. Guindet, M. Kleitz, *J. Electrochem. Soc.* **1997**, 144, 2427.
- [36] E. Mutoro, C. Hellwig, B. Luerssen, S. Guenther, W. G. Bessler, J. Janek, *Phys. Chem. Chem. Phys.* **2011**, 13, 12798.
- [37] A. K. Opitz, A. Lutz, M. Kubicek, F. Kubel, H. Hutter, J. Fleig, *Electrochim. Acta* **2011**, 56, 9727.
- [38] A. K. Opitz, M. P. Hörlein, T. Huber, J. Fleig, *J. Electrochem. Soc.* **2012**, 159, B502.
- [39] T. Huber, A. Opitz, J. Fleig, *Solid State Ionics* **2015**, 273, 8.
- [40] W. Jung, J. J. Kim, H. L. Tuller, *J. Power Sources* **2015**, 275, 860.
- [41] T. Keller, S. Volkov, E. Navickas, S. Kulkarni, V. Vonk, J. Fleig, A. Stierle, *Solid State Ionics* **2019**, 330, 17.
- [42] F. J. Norton, *J. Appl. Phys.* **1958**, 29, 1122.
- [43] R. Hartung, *Z. Phys. Chem.* **1975**, 256, 997.
- [44] L. R. Velho, R. W. Bartlett, *Metall. Mater. Trans. B* **1972**, 3, 65.
- [45] K. Sreenivas, I. Reaney, T. Maeder, N. Setter, C. Jagadish, R. G. Elliman, *J. Appl. Phys.* **1994**, 75, 232.
- [46] R. Schmiedl, V. Demuth, P. Lahnor, H. Godehardt, Y. Bodschiwinna, C. Harder, L. Hammer, H. P. Strunk, M. Schulz, K. Heinz, *Appl. Phys. A* **1996**, 62, 223.
- [47] T. Ryll, H. Galinski, L. Schlagenhauf, P. Elser, J. L. M. Rupp, A. Bieberle-Hutter, L. J. Gauckler, *Adv. Funct. Mater.* **2011**, 21, 565.
- [48] R. Stumpf, C. Liu, C. Tracy, *Appl. Phys. Lett.* **1999**, 75, 1389.
- [49] K. Chenoweth, A. C. Van Duin, W. A. Goddard, *J. Phys. Chem. A* **2008**, 112, 1040.
- [50] D. Fantauzzi, J. Bandlow, L. Sabo, J. E. Mueller, A. C. van Duin, T. Jacob, *Phys. Chem. Chem. Phys.* **2014**, 16, 23118.
- [51] J. P. Perdew, K. Burke, M. Ernzerhof, *Phys. Rev. Lett.* **1996**, 77, 3865.
- [52] G. Kresse, J. Hafner, *Phys. Rev. B* **1993**, 47, 558.
- [53] G. Kresse, J. Furthmüller, *Phys. Rev. B* **1996**, 54, 11169.
- [54] G. Kresse, J. Furthmüller, *Comput. Mater. Sci.* **1996**, 6, 15.
- [55] G. Kresse, D. Joubert, *Phys. Rev. B* **1999**, 59, 1758.
- [56] N. Wiberg, E. Wiberg, A. Holleman, *Lehrbuch der Anorganischen Chemie*, Vol. 102, Walter de Gruyter, Berlin, Germany **2007**.
- [57] P. Ehrhart, in *Landolt-Börnstein – Group III Condensed Matter – Atomic Defects in Metals* (Ed. H. Ullmaier), Vol. 25, Springer-Verlag, Berlin, Germany **1991**, pp. 256–262.
- [58] Y. Kraftmakher, *Phys. Rep.* **1998**, 299, 79.
- [59] J. P. Perdew, Y. Wang, *Phys. Rev. B: Condens. Matter Mater. Phys.* **1992**, 45, 13244.
- [60] T. R. Mattsson, A. E. Mattsson, *Phys. Rev. B: Condens. Matter Mater. Phys.* **2002**, 66, 214110.
- [61] B. Medasani, M. Haranczyk, A. Canning, M. Asta, *Comput. Mater. Sci.* **2015**, 101, 96.
- [62] G. Henkelman, B. P. Uberuaga, H. Jonsson, *J. Chem. Phys.* **2000**, 113, 9901.
- [63] G. Henkelman, H. Jonsson, *J. Chem. Phys.* **2000**, 113, 9978.
- [64] K. Momma, F. Izumi, *J. Appl. Crystallogr.* **2011**, 44, 1272.
- [65] S. Grimme, J. Antony, S. Ehrlich, H. Krieg, *J. Chem. Phys.* **2010**, 132, 154104.
- [66] S. Grimme, S. Ehrlich, L. Goerigk, *J. Comput. Chem.* **2011**, 32, 1456.
- [67] A. Stukowski, *Modell. Simul. Mater. Sci. Eng.* **2009**, 18, 015012.
- [68] H. M. Aktulga, J. C. Fogarty, S. A. Pandit, A. Y. Grama, *Parallel Comput* **2012**, 38, 245.
- [69] H. M. Aktulga, C. Knight, P. Coffman, K. A. O'Hearn, T. Shan, W. Jiang, *Int. J. High Perform. Comput. Appl.* **2019**, 33, 304.
- [70] S. Plimpton, *J. Comput. Phys.* **1995**, 117, 1.
- [71] D. Fantauzzi, J. E. Mueller, L. Sabo, A. C. Van Duin, T. Jacob, *ChemPhysChem* **2015**, 16, 2797.
- [72] D. Fantauzzi, S. Krick Calderon, J. E. Mueller, M. Grabau, C. Papp, H. Steinrück, T. P. Senftle, A. C. van Duin, T. Jacob, *Angew. Chem., Int. Ed.* **2017**, 56, 2594.
- [73] H. Monkhorst, J. Pack, *Phys. Rev. B* **1976**, 13, 5188.
- [74] P. Hirel, *Comput. Phys. Commun.* **2015**, 197, 212.
- [75] D. Krause, P. Thörnig, *J. Large-Scale Res. Facil.* **2018**, 4, A132.